



HAL
open science

Characterization of Li^+ Transport through the Organic-Inorganic Interface by using Electrochemical Impedance Spectroscopy

Agathe Naboulsi, Giao Nguyen, Sylvain Franger, Odile Fichet, Christel Laberty-Robert

► **To cite this version:**

Agathe Naboulsi, Giao Nguyen, Sylvain Franger, Odile Fichet, Christel Laberty-Robert. Characterization of Li^+ Transport through the Organic-Inorganic Interface by using Electrochemical Impedance Spectroscopy. *Journal of The Electrochemical Society*, 2024, 171 (2), pp.020523. 10.1149/1945-7111/ad2595 . hal-04578940

HAL Id: hal-04578940

<https://hal.science/hal-04578940v1>

Submitted on 6 Sep 2024

HAL is a multi-disciplinary open access archive for the deposit and dissemination of scientific research documents, whether they are published or not. The documents may come from teaching and research institutions in France or abroad, or from public or private research centers.

L'archive ouverte pluridisciplinaire **HAL**, est destinée au dépôt et à la diffusion de documents scientifiques de niveau recherche, publiés ou non, émanant des établissements d'enseignement et de recherche français ou étrangers, des laboratoires publics ou privés.

OPEN ACCESS

Characterization of Li^+ Transport through the Organic-Inorganic Interface by using Electrochemical Impedance Spectroscopy

To cite this article: Agathe Naboulsi *et al* 2024 *J. Electrochem. Soc.* **171** 020523

View the [article online](#) for updates and enhancements.

You may also like

- [Temperature Dependence of Dendritic Lithium Electrodeposition: A Mechanistic Study of the Role of Transport Limitations within the SEI](#)
Adam Maraschky and Rohan Akolkar
- [Carbon-Based Electrodes for Lithium Air Batteries: Scientific and Technological Challenges from a Modeling Perspective](#)
Alejandro A. Franco and Kan-Hao Xue
- [Quantifying Resistive and Diffusive Kinetic Limitations of Thiophosphate Composite Cathodes in All-Solid-State Batteries](#)
S. Yanev, H. Auer, R. Pertsch *et al.*

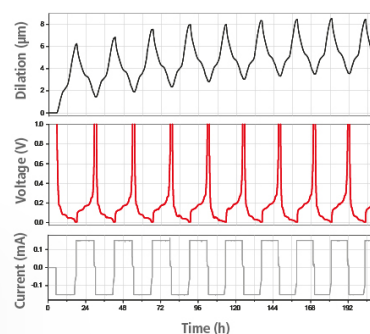
Watch Your Electrodes Breathe!

Measure the Electrode Expansion in the Nanometer Range with the ECD-4-nano.

- ✓ Battery Test Cell for Dilatometric Analysis (Expansion of Electrodes)
- ✓ Capacitive Displacement Sensor (Range 250 μm , Resolution ≤ 5 nm)
- ✓ Detect Thickness Changes of the Individual Half Cell or the Full Cell
- ✓ Additional Gas Pressure (0 to 3 bar) and Temperature Sensor (-20 to 80° C)



EL-CELL[®]
electrochemical test equipment



See Sample Test Results:



Scan me!

Download the Data Sheet (PDF):



Scan me!

Or contact us directly:


+49 40 79012-734

sales@el-cell.com

www.el-cell.com



Characterization of Li⁺ Transport through the Organic-Inorganic Interface by using Electrochemical Impedance Spectroscopy

Agathe Naboulsi,^{1,2,3} Giao T. M. Nguyen,¹ Sylvain Franger,⁴ Odile Fichet,¹ and Christel Laberty-Robert^{2,3,z} 

¹CY Cergy Paris Université, LPPI, F-95000 Cergy, France

²Sorbonne Université, CNRS, Laboratoire Chimie de la Matière Condensée de Paris, LCMCP, 4 Place Jussieu, 75005 Paris, France

³RS2E, Réseau Français sur le Stockage Electrochimique de l'Energie, CNRS 3459, 80039 Cedex 1 Amiens, France

⁴Université Paris-Saclay, CNRS, ICMO-ERIEE (UMR 8182), 17 avenue des Sciences, 91400 Orsay, France

Understanding Li⁺ transport at polymer/inorganic interfaces is crucial for developing composite electrolytes in solid-state batteries. In our investigation, we employed impedance spectroscopy and established a multilayer methodology for assessing Li⁺ transport at this interface. The inorganic phase chosen was Li_{6.25}Al_{0.25}La₃Zr₂O₁₂ (Al-LLZO), and the organic phase comprised a Poly(ethylene oxide) (PEO) network with dangling chains. Li⁺ incorporation in the polymer, as a free either salt or associated with anion grafting onto the PEO network, was explored. Additionally, the PEO network was either pressure-adhered to the inorganic surface (ex-situ configuration) or synthesized onto the Al-LLZO surfaces (in situ configuration) to investigate processing effects on Li⁺ transport. Using a Transmission Line Model for impedance data analysis, our study identified two key elements governing Li⁺ transport at the interface: R_i, representing resistance along the ionic pathway, and R_c and C_d, describing distributed resistance and capacitance within the interface. We observed that R_i is influenced by the polymerization process in the presence of Al-LLZO ceramic, while R_c remains constant regardless of the synthesis method. This suggests varying Li⁺ concentrations at the interphase in the in situ configuration, while interface/interphase heterogeneity remains consistent across configurations. The estimated activation energy indicates more energetically favorable direct Li⁺ transport in the in-situ configuration.

© 2024 The Author(s). Published on behalf of The Electrochemical Society by IOP Publishing Limited. This is an open access article distributed under the terms of the Creative Commons Attribution 4.0 License (CC BY, <http://creativecommons.org/licenses/by/4.0/>), which permits unrestricted reuse of the work in any medium, provided the original work is properly cited. [DOI: 10.1149/1945-7111/ad2595]



Manuscript submitted December 10, 2023; revised manuscript received January 9, 2024. Published February 14, 2024.

Supplementary material for this article is available [online](#)

All-solid-state lithium batteries (ASSBs) represent the next generation of electrochemical energy storage devices, primarily due to their safety and their high energy density, reaching up to 400 Wh kg⁻¹. The integration of Li metal as the negative electrode plays a pivotal role in achieving these remarkable attributes. Within the realm of ASSBs, the electrolyte stands out as a critical component, yet none of the existing electrolyte families currently available fully satisfies all the essential requirements, which encompass ionic conductivity, processability, as well as electrochemical and chemical stability with respect to Li.¹ In this context, the design of composite materials emerges as the most promising solution in the short term.² In the realm of electrolyte design, a common trade-off is observed: incorporating a polymer enhances electrolyte processability but often comes at the cost of reduced ionic conductivity. In contrast, inorganic materials demonstrate enhanced ionic conductivity at the expense of decreased processability. A significant challenge when designing composite materials lies in the tuning of the inorganic/organic interface, as it governs several critical properties, including the transport of Li⁺ ions. To create the ideal composite material, a crucial prerequisite is a thorough comprehension of the experimental parameters that enhance effective Li⁺ ion transport across this interface.^{3,4} To the best of our knowledge, there have been relatively few studies focusing on understanding Li⁺ transport at the polymer electrolyte/inorganic interface where the polymer electrolyte is generally composed of a Lithium salt solubilized in linear poly(ethylene oxide) (PEO—Li salt polymer). Zheng et al.⁵ demonstrated by NMR analysis that the content of Lithium lanthanum zirconate (Li₇La₃Zr₂O₁₂, LLZO) in their composite with PEO-LiTFSI polymer, obtained by solution casting, significantly impacts ion mobility. On one hand, when the composite contains a high mass fraction of polymer (80–95 wt%), it exhibits ionic conductivity similar to that of the polymer itself (~10⁻⁵ S.cm⁻¹). On the other hand, a high mass fraction of LLZO

(≥50 wt%) results in lower ionic conductivity (10⁻⁶–10⁻⁷ S.cm⁻¹), attributed to poor LLZO||LLZO interface that restricts Li⁺ ion transport within the inorganic percolated network. To elucidate this phenomenon, several hypotheses have been proposed, including changes in the transport mechanism along or through the LLZO||polymer interface. Brogioli et al.⁶ explored the latter through the estimation of the activation energy of the ionic conduction at the interface using impedance spectroscopy. Interestingly, they estimated a high activation energy barrier for Li⁺ between the two phases (LLZO—PEO), indicating the challenge that Li⁺ ions face when moving from one phase to the other. To overcome this limitation, Kuhnert et al.⁷ investigated surface modification by covalently grafting PEO chains to Li_{6.4}La₃Zr_{1.4}Ta_{0.6}O₁₂ (LLZTO) particles. To archive this, the surface-terminated oxygen groups on the LLZTO particles is activated by plasma etching. Subsequently, (3-glycidyloxypropyl)trimethoxysilane (Si—R) was grafted on the LLZTO surface via plasma-activated oxygen resulting in particles functionalized with oxirane group. These oxirane groups were then reacted with the hydroxyl-terminated PEOs, enabling surface functionalization with PEO chains. Interestingly, this functionalization induces changes in the surface charge properties of LLZTO. As a result, the PEO segments self-organize around the LLZTO particles, leading to a significant reduction in the distance that Li⁺ ions need to traverse between LLZTO and the PEO polymer. This reduction, in turn, facilitates the smooth transfer of Li⁺ ions across the LLZTO||PEO interface, as evidenced by a decrease of the resistance measured by impedance spectroscopy.

To quantify the interface resistance, Gupta et al.⁸ designed a multilayer PEO—LiTFSI||LLZTO||PEO—LiTFSI system and studied the Li⁺ transport through these multilayers by impedance spectroscopy. In their studies, the impedance spectra exhibit two distinct frequency-dependent phenomena on the Nyquist representation, corresponding to two semi-circles. The high frequency (HF) semi-circle is attributed to the bulk response corresponding to both the resistance of the PEO—LiTFSI polymer and the bulk LLZTO. The second one, at a medium frequency (MF), is attributed to the interface and noted R_{interface}. For determining,

^zE-mail: christel.laberty@sorbonne-universite.fr

the value of $R_{\text{interface}}$, they used the following electronic circuit model: $(CPE_{\text{bulk}}/R_{\text{bulk}}) + (CPE_{\text{interface}}/R_{\text{interface}}) + M_{\text{Au}}$. $CPE_{\text{bulk}}/R_{\text{bulk}}$ accounts for the combined capacitance and resistance of the bulk layers of the three electrolytes, while $CPE_{\text{interface}}/R_{\text{interface}}$ represents the capacitance and resistance between the two electrolytes. Finally, M_{Au} represents the capacitive effect arising from the presence of blocking gold electrodes. They estimated a $R_{\text{interface}}$ of $15 \text{ k}\Omega\cdot\text{cm}^2$ at 30°C , noting a reduction in this value when the LLZTO surface was cleaned through heat treatment ($0.2 \text{ k}\Omega\cdot\text{cm}^2$) and when the Li^+ concentration within the polymer electrolyte was adjusted. Indeed, increasing the Li^+ concentration in the polymer caused a shift in the concentration gradient between the two electrolytes, thereby facilitating the transport of Li^+ ions. These findings align with similar observations made in multilayer systems involving $\text{Li}_{1-x+y}\text{Al}_x\text{Ti}_{2-x}\text{Si}_y\text{P}_{3-y}\text{O}_{12}$.⁹ Using a methodology comparable to Gupta et al.,⁸ they demonstrated that the interfacial resistance, $R_{\text{interface}}$, is inversely proportional to the concentration of Li^+ in the polymer, within the range of concentration of $0.01\text{--}2.5 \text{ M}$ ($R_{\text{interface}} \sim 2.10^3 \Omega\cdot\text{cm}^2$ and $20 \Omega\cdot\text{cm}^2$, respectively at 30°C and 70°C). Interestingly, Langer et al.¹⁰ observed an additional ion transfer process attributed to interface processes on $\text{PEO-LiClO}_4\|\text{LLZO}\|\text{PEO-LiClO}_4$ multilayers. To better understand and quantify its impact on the overall behavior, they incorporated a de Levie element into their equivalent circuit: $R_{\text{SE}} + Z_{\text{deLevie}} + CPE_{\text{dl}}$. In this model, R_{SE} characterizes the combined resistance of the electrolytes, Z_{deLevie} describes the porous structure at the interface between the two electrolytes, and CPE_{dl} represents the capacitance at the blocking electrodes. Using Z_{deLevie} for porous electrodes is a standard procedure for discerning between the transports of Li^+ ions within the pores and their ionic transfer across the phase boundary.^{11,12} Under these conditions, a $R_{\text{interface}}$ of $9 \text{ k}\Omega\cdot\text{cm}^2$ was estimated at 70°C . Notably unlike the previous studies,^{8,9} this model describes the heterogeneities present at the interface via a de Levie element.

Drawing inspiration from these existing literature studies, we propose an alternative approach to create a multilayer system consisting of $\text{LiTFSI-PEO network}\|\text{Al-LLZO}\|\text{LiTFSI-PEO network}$, leveraging our understanding of the polymerization process of PEO networks from liquid monomers.¹³ This methodology allows us to investigate the impact of processing onto Li^+ transfer at the $\text{Al-LLZO}\|\text{LiTFSI-PEO}$ interface. Firstly, a two-step assembly approach is employed, involving the synthesis of the polymer followed by its assembly onto the Al-LLZO ceramic through pressure, referred to the ex situ approach. Secondly, the polymerization of the PEO network is conducted directly onto Al-LLZO ceramics, named the in-situ approach. Notably, in our synthesis approach for PEO, lithium counterions can be grafted to polymer chains by utilizing the lithium 3-[(trifluoromethane)sulfonamidofonyl] propyl methacrylate (MTFSI, see Fig. S1 for chemical formula) monomer as a substitute for LiTFSI. This provides control over the diffusion of Li^+ at the interfaces.¹³ Contrary to previous studies, the LiTFSI-PEO and LiMTFSI-PEO networks, synthesized directly on the Al-LLZO pellet surface using liquid monomers, are amorphous across a wide temperature range. This novel approach is expected to yield a distinct interface compared to traditional linear PEO. Notably, these LiTFSI-PEO and LiMTFSI-PEO networks exhibit conductivity values of $10^{-5} \text{ S}\cdot\text{cm}^{-1}$ and $10^{-7} \text{ S}\cdot\text{cm}^{-1}$, respectively, at 25°C ^{13,14} lower than the measurement on dense $\text{Li}_{6.4}\text{La}_3\text{Zr}_2\text{Al}_{0.2}\text{O}_{12}$ ceramic ($10^{-4} \text{ S}\cdot\text{cm}^{-1}$ at 25°C).¹⁵

The results of the different multilayers were discussed with respect to the processing methods (in-situ vs ex-situ for $\text{LiTFSI-PEO network}$) and the diffusion of Li^+ (MTFSI vs LiTFSI). To analyze our impedance data and understand the transport phenomena at the interfaces, we incorporated a Transmission Line Model (TLM) into the equivalent circuit. This element takes into account the heterogeneities present at the interface, both chemical and microstructural. Compared to the de Levie model, which proposes a series/parallel equivalent circuit comprised of a distribution of ohmic (resistive) and capacitive elements, leading to modeling the entire electrode with a non-uniform effective resistance and capacitance,

our system is different. In our system, only the transfer of Li^+ from one electrolyte to the other occurs. Therefore, we propose a TLM element, considering the ohmic drop due to the mobility of Li^+ in the interphase (R_i that correspond to the homogeneous transport inside the interphase) in series with a ohmic drop due to heterogeneity within the interface (R_i corresponding to exchange pathway for Li^+ between both electrolytes) in parallel with the space charge capacitance (C_i , created between both electrolytes from the existing dielectric strength). Interestingly, Euler and Nonnenmacher initially introduced TLM to clarify the hindered diffusion of Li^+ within the pores of porous Li-ion electrodes that are filled with a liquid electrolyte.¹⁶

Experimental

Materials.— $\text{Li}_{6.25}\text{Al}_{0.25}\text{La}_3\text{Zr}_2\text{O}_1$ (Al-LLZO , 400 to 600 nm D50, Ampcera) and Lithium bis(trifluoromethylsulfonyl)imide (LiTFSI, >99%, Sigma Aldrich) was kept in the glove box ($\text{H}_2\text{O} < 0.1 \text{ ppm}$). Poly(ethylene glycol) methyl ether methacrylate (PEGM, $M_n = 500 \text{ g}\cdot\text{mol}^{-1}$, Sigma Aldrich), poly(ethylene glycol) dimethacrylate (PEGDM, $M_n = 750 \text{ g}\cdot\text{mol}^{-1}$, Sigma Aldrich) and lithium 3 [(trifluoromethane)sulfonamidofonyl] propyl methacrylate (LiMTFSI, Specific Polymer) were dried at 25°C under vacuum (10^{-15} mbar) before used. 2,2'-azobis(2-methylpropionitrile) (AIBN, initiator, 98%, Sigma Aldrich) was recrystallized in methanol before used. For the synthesis of Li_3BO_3 (LBO), H_3BO_3 (Alfa Aesar) and LiOH (Alfa Aesar) have been used in stoichiometric proportion.

Materials Synthesis

Synthesis procedure for Al-LLZO ceramics.—LBO was first synthesized by dissolving H_3BO_3 and LiOH into distilled water in a 1:3 molar ratio and stirred vigorously at 50°C to make a homogeneous solution. The solution was then dried at 120°C with stirring under low rpm. The resulting powder was finally heat-treated at 600°C for 12 h to obtain LBO. Al-LLZO ceramics were obtained from commercial Al-LLZO powder manually ground with 5 wt% of LBO. 1 g of the ground powder mixture was then pressed under 296 MPa to achieve 13 mm diameter pellets. Excess of lithium source was adopted to compensate for the lithium loss (volatilization) during sintering. To do so, the pellets were covered in an Al_2O_3 crucible with commercial Al-LLZO powder. These pellets were then sintered under air in an alumina crucible with a heating rate of $5^\circ\text{C}\cdot\text{min}^{-1}$ at 780°C during 5 h and then with a heating rate of $1^\circ\text{C}\cdot\text{min}^{-1}$ at 1150°C for 12 h in a muffle furnace. The sintered pellets exhibit a thickness of $\sim 0.2 \text{ cm}$ and a diameter of $\sim 1.0\text{--}1.2 \text{ cm}$. The relative density is about 90%.

Synthesis procedure of polymer networks.—Polymer electrolyte syntheses were performed as previously reported in Naboulsi et al.¹³ For $\text{LiTFSI/polymer network}$, PEGM and PEGDM (ratio PEGM/PEGDM: 80/20 wt/wt) and 2 wt% AIBN by respect to the total monomer weight were introduced into a vial. The precursor solution was stirred until the total solubilization of AIBN then flushed with nitrogen. The vial was then introduced in a glove box ($\text{H}_2\text{O} < 0.1 \text{ ppm}$). Finally, 18 wt% of LiTFSI ($\text{EO/Li} = 24$) was added to the PEGM/PEGDM solution and stirred until the LiTFSI was completely dissolved.

For single-ion polymer electrolyte, PEGM and PEGDM (ratio PEGM/PEGDM: 80/20 wt%) and 21 wt% LiMTFSI ($\text{EO/Li} = 24$) were introduced in a vial and stirred until the total solubilization of LiMTFSI (2 h) at room temperature. 2 wt% of AIBN concerning the total weight of PEGM, PEGDM and LiMTFSI were added to the mixture, which was then stirred and flushed with nitrogen until the AIBN was dissolved.

For the synthesis of the polymer networks, the previous mixtures were poured into a mold made with two glass plates separated by a Teflon gasket (thickness $\sim 0.025 \text{ cm}$). The mold was then placed in

an oven at 70 °C for 2 h and then at 90 °C for 1 h. The resulting polymer networks were then dried under vacuum (10–15 mbar) at 70 °C in a glass oven (BUCHI B-585) for 12 h and then kept in a glove box ($H_2O < 0.1$ ppm) before use.

The obtained materials (LiTFSI-PEO network and LiMTFSI-PEO network) are soft and flexible with soluble fractions in methanol of 21 wt% (including 18 wt% of LiTFSI) and 2 wt% respectively, attesting the successful formation of polymer networks.¹³

Synthesis of the (PEO network||Al–LLZO||PEO network) multilayers.—Two different approaches have been used for the fabrication of the multilayers to control Al–LLZO||polymer interface. As a first approach, the polymer layer was synthesized on the surface of the Al–LLZO pellet; this approach will be called in-situ in the rest of the manuscript. In the glove box, the Al–LLZO pellet surface was first cleaned on both sides with silicon carbide sanded polishing paper to avoid the presence of carbonate phases.^{17,18} A volume of about 10 μ l of the chosen precursor mixture was spread with a micropipette on one whole side of the pellet (0.99 cm²) to achieve a final thickness of around 0.02 cm. On a hot plate in glove box, a thermal curing of 2 h at 70 °C, followed by a post-curing of 1 h at 90 °C was applied to obtain the Al–LLZO/polymer bilayer assembly. The assembly was then cooled to room temperature. The second polymer layer was synthesized on the uncovered side of the Al–LLZO with the same procedure leading to a multilayer assembly PEO network||Al–LLZO||PEO network, and called in-situ multilayer in the rest of the manuscript.

In a second approach, two polymer films (thickness of ~ 0.25 mm) were first prepared as previously described (i.e., the synthesis procedure of the polymer network). They were assembled with an Al–LLZO pellet to form the configuration of PEO network||Al–LLZO||PEO network in a Swagelok cell, and the contact was maintained with a spring (0.4 MPa). This approach is called ex-situ in the rest of the manuscript. The two approaches for multilayers are described in Fig. 1 and Table SI. Multiple multilayer tests were carried out to assess reproducibility, with the discussion focusing on three representative selected samples.

Testing procedure.—The multilayers (in-situ and ex-situ) and polymer electrolyte were then placed in a Swagelok-type cell using two stainless-steel blocking electrodes (BE). A metallization with 50 nm Au was performed for Al–LLZO pellet and PEO-like network to ensure good contact. In this configuration, Au is used as blocking electrode. In all the cells, contact was made through a spring (0.4 MPa).

Characterization

Electrochemical impedance spectroscopy (EIS) experiments were carried out using a 1260 Solartron FRA device between 10⁷ Hz and 10⁻¹ Hz, with a perturbation amplitude of 100 mV at the OCV (open circuit voltage), recording 11 points per decade. The activation energy was estimated from the complex impedance spectra measured every 10 °C from 30 °C to 80 °C. Temperature was controlled using an environmental simulation chamber (Mettler). Cells were allowed to reach the thermal equilibrium

for at least 1 h before each measurement. The fit of the experimental data was performed using Zview software.

Calculation of the capacitance from the constant phase element (CPE).—Using the Zview software for the impedance data refinement, the CPE element includes two components, CPE and α , respectively. The equivalent capacitance is calculated according to the following equation:¹⁹

$$C = \frac{(CPE * R)^{\frac{1}{\alpha}}}{R} \quad [1]$$

with R, the resistance in parallel to the CPE element in the electrical equivalent circuit.

Results and Discussion

To understand Li⁺ ion transport in composite electrolytes, it is crucial to investigate how Li⁺ ions move at the interface between the PEO network and Al–LLZO ceramics. To achieve this, we initially developed multilayers comprising. Two distinct approaches were explored to tune the LiTFSI–PEO network||Al–LLZO interface. In the in situ approach, the PEO network layer is directly synthesized on the surface of Al–LLZO ceramics, while in the ex-situ approach, the LiTFSI–PEO network layer is initially synthesized and then maintained by pressure onto the Al–LLZO surface. Electrochemical Impedance Spectroscopy (EIS) was used to characterize the Li⁺ transport^{20,21} and all EIS measurements were realized in a Swagelok-type cell and contacts were maintained with a constant pressure of 0.4 MPa using a spring.

Before studying the different multilayers, we have independently characterized the Li⁺ transport in the individual electrolytes (LiTFSI–PEO network and Al–LLZO ceramic) by using an Aulelectrolyte cell configuration (where gold is acting as an ion-blocking electrode, BE). The results are reported in Fig. 2. For all the temperatures, the values of the different electrical elements used in the model are summarized in Tables SII and SIII for the PEO based networks and Al–LLZO, respectively. According to the literature,²⁰ the BE||LiTFSI–PEO network||BE impedance spectra can be divided into two parts (Fig. 2a).

The High Frequency response is influenced by the ionic motion within the material, while the low frequency (LF) component is predominantly dictated by electrode polarization. When a low-frequency perturbation signal is applied, Li⁺ and TFSI ions tend to accumulate at the interface with the blocking electrodes. This accumulation results in a reduction of positive charges on the opposing metallic electrodes. The resistance of the LiTFSI–PEO network, $R_{polymer}$ and its capacitance, $CPE_{polymer}$ were determined from the impedance data by fitting the spectra according to the equivalent circuit in the inset. Figure 2a shows selected sample and fitted spectra, where CPE was used to take into account the non-ideality of the capacitors (described in the method). More precisely, this fitting was achieved using the classical $R_{swagelok} + CPE_{polymer} // (R_{polymer} + CPE_{BE})$ Debye equivalent circuit, as shown in the inset of Fig. 2a. Additionally, $R_{swagelok}$ represents the resistance of the entire setup (cell, cables), while CPE_{BE} characterizes the capacitive response from the blocking electrodes. From the modeling of the impedance data of the LiTFSI

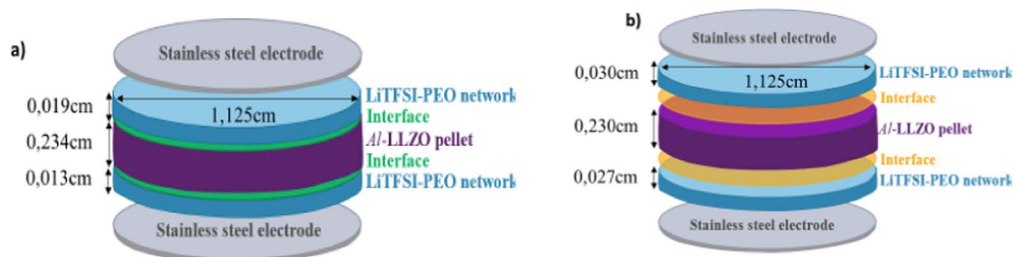


Figure 1. Schematic representation of (a) in-situ LiTFSI–Multilayer, (b) ex-situ LiTFSI–Multilayer.

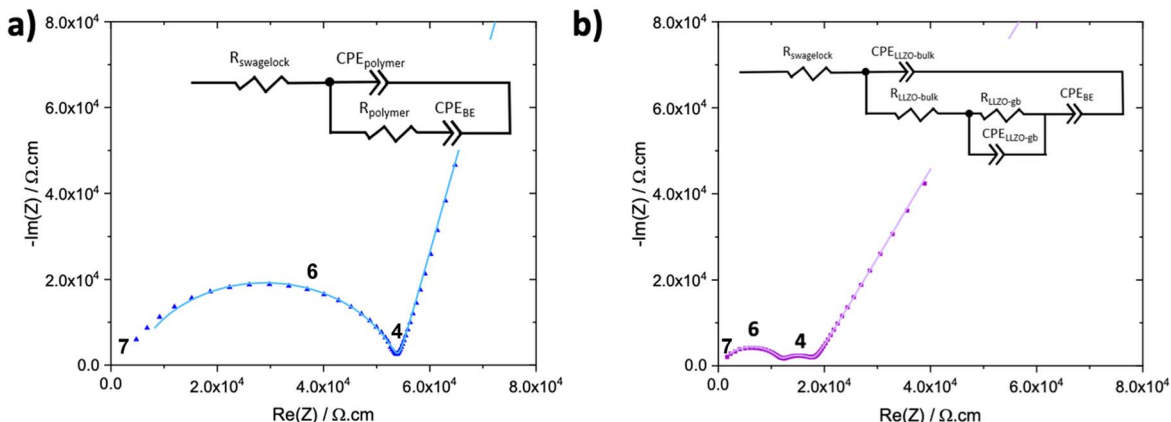


Figure 2. Nyquist plot at 30 °C of (a) BE||LiTFSI—PEO network||BE, (b) Au||Al—LLZO||Au and (—) fit according to the equivalent circuit presented. Numbers at the data points indicate power of frequency.

Table I. Values of electrical circuit elements at 30 °C for BE||LiTFSI—PEO network||BE, BE||MTFSI—PEO network||BE and Au||Al—LLZO||Au.

Sample	$R_{LLZO-bulk}$ or polymer (Ω)	$C_{LLZO-bulk}$ or polymer ($F.cm^{-2}$)	$R_{LLZO-gb}$ (Ω)	$C_{LLZO-gb}$ ($F.cm^{-2}$)	Conductivity ($S.cm^{-1}$) at 30 °C
Al—LLZO	2830	2.10^{-11}	1306	7.10^{-9}	5.6×10^{-5}
LiTFSI—PEO network	1700	6.10^{-11}			1.9×10^{-5}
LiMTFSI—PEO network	95327	$1.3.10^{-10}$			4×10^{-7}

—PEO network using the classical equivalent circuit, a capacitance value of $6.10^{-11} F.cm^{-2}$ (Eq. 1) and a conductivity value of $1.9.10^{-5} S.cm^{-1}$ at 30 °C were estimated (Table I).

In Fig. 2b, the impedance spectra of the Au||Al—LLZO||Au cell is reported and reveals three distinct regions. The corresponding equivalent circuit is represented in the inset. According to the literature, the first semi-circle at HF is associated with the motion of Li^+ ion within the bulk Al—LLZO grains. The capacitance for these regions, estimated at $2.10^{-11} F.cm^{-2}$ (see Table I) calculated using Eq. 1, has been determined based on the $CPE_{LLZO-bulk}$ estimated from the fit of the impedance diagram with the equivalent circuit represented in the inset. The second semicircle at medium frequency (MF) corresponds to the grain boundaries (GB) response with a capacitance of $7.10^{-9} F.cm^{-2}$ (Table I). Finally, the capacitive response, CPE_{BE} , observed at LF is attributed to the Al—LLZO||Au blocking interface. By considering the bulk and grain boundaries resistances, an effective ionic conductivity of $5.6 \times 10^{-5} S.cm^{-1}$ was estimated for our Al—LLZO ceramic. This value differs from the $10^{-4} S.cm^{-1}$ usually reported in the literature due to the relative density of our pellet (close to 90%).

We have then studied the in-situ LiTFSI—Multilayer by impedance spectroscopy with the same setup configuration and the experimental data (represented in a Nyquist plot) are reported in Fig. 3.

The impedance spectrum of this multilayer exhibits four different zones: a semi-circle at HF (10^7 – 10^5 Hz, zone a), a contribution at HF—MF (3.10^4 Hz, zone b) followed by a shoulder at MF (zone c), and a capacitive response at LF (zone d) corresponding to the charge accumulation at the blocking electrode surface (modeled by CPE_{BE}). The HF response (zone a) was attributed to the transport of Li^+ into both the LiTFSI—PEO network and Al—LLZO, according to the apparent frequency of the two reference cells for both individual electrolytes ($\sim 10^5$ Hz) (see Figs. 2a and 2b). Accordingly, the HF—MF region corresponds to the grain boundaries response of the Al—LLZO (zone b), as the apparent frequency (3.10^4 Hz) corresponds to the one found for Al—LLZO GB (see Fig. 2b). These different features are modeled by $R_{swagelock} + [(R_{polymer} + CPE_{BE}) / CPE_{polymer}] + [R_{LLZO-bulk} + (R_{LLZO-gb} /$

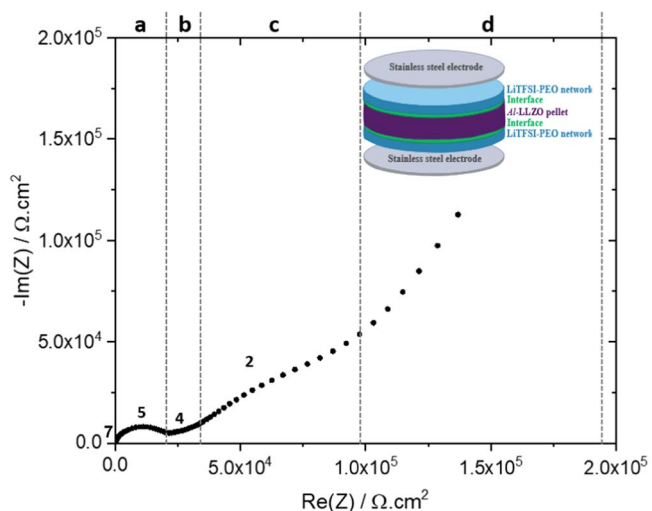


Figure 3. Nyquist plot at 30 °C of in-situ LiTFSI—Multilayer and its schematic representation. Numbers at the data points indicate the power of frequency. (a)–(d) on top of the Nyquist plot represent the different frequency zones.

$CPE_{LLZO-gb} / CPE_{LLZO-bulk}$]. Interestingly, the MF contribution (zone c) that coincides with the Al—LLZO—gb is also attributed to the LiTFSI—PEO network||Al—LLZO interface. This assignment is made because of the fitting of the impedance spectra using solely the two electrolytes in series provides an inadequate fit (sum of square = 200), as demonstrated in Fig. 4a.

According to Isaac et al., a resistance in parallel with a constant phase element models this latter contribution.⁹ Using the equivalent circuit reported in Fig. 4b, the fit with the experimental data demonstrates good agreement in the zones a and b (sum of square = 40). However, the fit is poor in zone c, possibly due to a non-ideal or more complex interface in our specific case.

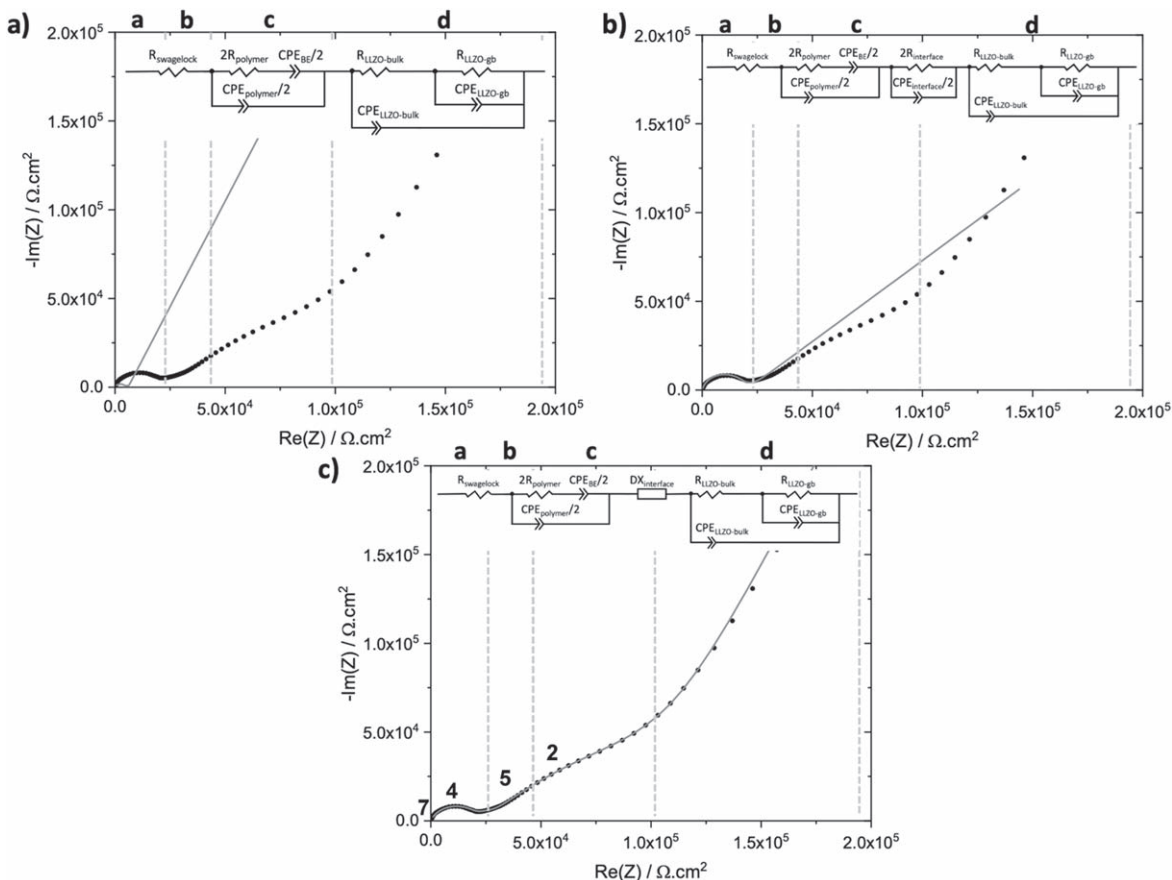


Figure 4. Nyquist plot at 30 °C of (●) in-situ LiTFSI—Multilayer, (—) fit according to the equivalent circuit presented respectively on each graph. a, b, c and on top of the Nyquist plot represent the different frequency zones. Note that the equivalent circuits presented in the insert are written with 2 R and CPE/2 to take into account that the multilayer is made of two polymer layers. Numbers at the data points indicate the power of frequency.

In order to better describe the heterogeneity of our LiTFSI—PEO network||Al—LLZO interface, both in terms of morphology (possible dense and porous zones) and chemistry (possible distribution of conductive and insulating zones), we propose replacing the last contribution with a TLM, represented as DX element in the software, within our equivalent circuit (refer to Fig. 4c). This approach has been extensively used in porous electrode of Li-ion batteries to model the diffusion/transfer of Li⁺ ions. In classical TLM (see Fig. S2), R_i reflects the percolated ionic path within the pores of the electrode filled with liquid electrolyte while R_{ct} and C_{dl} represent the charge transfer resistance and the double layer capacitance.²⁰ Inspiringly, in our hybrid interface, where only Li⁺ ions diffuse through it, we assigned R_i to the resistivity of the direct ionic path at the LiTFSI—PEO network||Al—LLZO interface, particularly within the percolated ionic conductive regions in our DX. Conversely, R_t and C_t signify the distributed resistance and capacitance, representing the distributed resistivity and permittivity, within the heterogeneous structure of this “hybrid” interface. The introduction of this additional distributed R_t/C_t element emphasizes a more intricate, tortuous, and unfavorable pathway (polarization) for Li⁺ ions. The equivalent circuit shown in Fig. 4c is then proposed and has been used to fit our experimental data. As shown in the same figure, the fit is remarkably consistent with our experimental results (sum of square = 0.24).

The LiTFSI—PEO network||Al—LLZO interfacial resistance of in-situ LiTFSI—Multilayer at 30 °C has then been evaluated to be ~8.0 kΩ.cm², taking into account that the interfacial resistance corresponds to R_i in the TLM element. This value is higher than the one (R_{interface} = 0.2 kΩ.cm²) estimated by Gupta et al.⁸ on PEO—LiTFSI||LLZTO||PEO—LiTFSI multilayer using a classical R/C equivalent circuit. The key distinction between their investigation

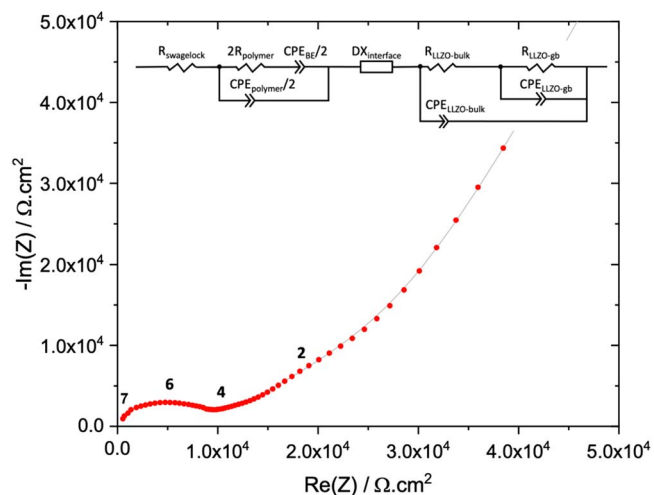


Figure 5. Nyquist plot at 30 °C of (●) ex-situ LiTFSI—Multilayer, (—) fit according to the equivalent circuit presented. Numbers at the data points indicate the power of frequency.

and our research pertains to the composition of the LiTFSI—PEO organic phase. In their study, it relies on linear PEO at a high concentration of LiTFSI ([OE]/[Li] = 15), whereas in our case, it is cross-linked with a lower Li⁺ concentration ([OE]/[Li] = 24). Moreover, the processing of the multilayer differs significantly. Specifically, it involves either stacking and hot pressing pre-formed layers or the in situ polymerization of the LiTFSI—PEO polymer on the surface of the Al—LLZO in our study.

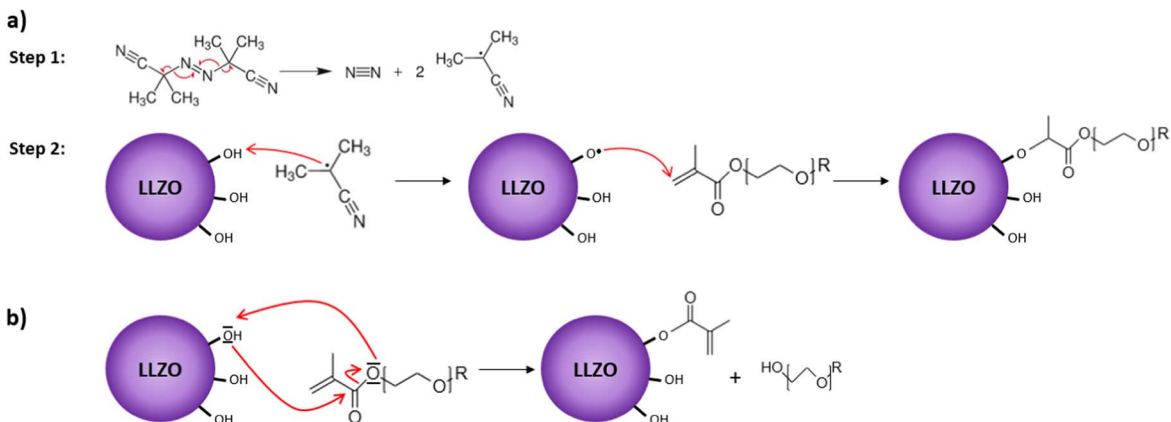


Figure 6. (a) Hypothesis on the reaction between PEO network precursors and *Al*-LLZO activated by the free radicals from AIBN, (b) Hypothesis on the reaction between *Al*-LLZO and methacrylate from PEO network precursor.

To examine whether the fabrication process leads to variations in the resistance of the LiTFSI-PEO network|*Al*-LLZO interface, we conducted a study on an ex-situ LiTFSI-Multilayer, by stacking the pre-formed layers and held under moderated pressure (0.4 MPa) during the electrochemical tests. The shape of the impedance plot (Fig. 5) is similar to the one obtained for in-situ polymerization. Therefore, we employed the identical equivalent circuit as depicted in Fig. 4c, and the results are illustrated in Fig. 5, affirming that this circuit accurately models our data.

The modeling results yield the values of R_i and R_t for all investigated temperatures, compiled in Table SIV for in-situ LiTFSI-Multilayer and Table SV for ex-situ LiTFSI-Multilayer. In the case of the ex-situ LiTFSI-Multilayer, the composite interface exhibits a resistance R_i of approximately $1.2 \text{ k}\Omega\cdot\text{cm}^2$ at 30°C . This value is significantly lower than the observed resistance for the in-situ LiTFSI-based multilayer ($8.0 \text{ k}\Omega\cdot\text{cm}^2$). The primary distinction between the two multilayers lies in the fact that the LiTFSI-PEO network is formed in-situ, allowing for covalent bonding between PEO precursors and the *Al*-LLZO ceramic through two distinct mechanisms (depicted in Fig. 6). In the first mechanism, free radicals originating from the initial polymerization state have the capacity to transfer to the hydroxyl group on the surface of the *Al*-LLZO ceramic. Subsequently, the resultant radical can initiate both polymerization and the grafting of PEGM or PEGDM onto the ceramics, as illustrated in Fig. 6a. In the second mechanism, transesterification may take place between the methacrylate group of the PEO network's precursor (PEGM or/and PEGDM) and the hydroxyl group on the surface of the *Al*-LLZO

(refer to Fig. 6b). The grafted methacrylate function can then actively contribute to the creation of a PEO network grafted onto the surface of *Al*-LLZO. This covalent bonding will probably modify the organization of the PEO chain at the surface of the *Al*-LLZO and eventually the concentration of Li^+ at the interface. FTIR spectroscopy analyses were conducted to confirm the hypothesis of a covalent bond between the PEO network and the *Al*-LLZO ceramic. Unfortunately, the concentration of the PEO chain grafted onto the ceramic surface is likely too small to be detected, possibly owing to the 2D morphology of the interface.

The in-situ formation of the PEO network appears to be less favorable to the direct transport of Li^+ at the LiTFSI-PEO network|*Al*-LLZO interface across the entire temperature range, as evidenced by the in-situ multilayer's R_i being at least one order of magnitude higher than that of the ex-situ multilayer (see Fig. 7a). However, this trend is not observed in the distributed phenomena described by R_i/C_i in the TML element (see Fig. 7b). R_i/C_i represents the distribution of conductivity and permittivity within the interface thickness, with its value predominantly influenced by the chemistry of this hybrid layer. The similarity in R_i for both in-situ and ex-situ multilayers suggests that the "bulk" chemistry is likely identical. Furthermore, this implies that in-situ polymerization only modifies the chemistry at the interface (presence of an interphase). The noted variation in R_i between the in situ and ex situ polymerization approaches suggests that the PEO chains directly grafted onto the *Al*-LLZO surface lead to a distinct concentration of Li^+ at the interface. This divergence is attributed to the presence of methacrylate groups, which are less favorable for Li^+ ion

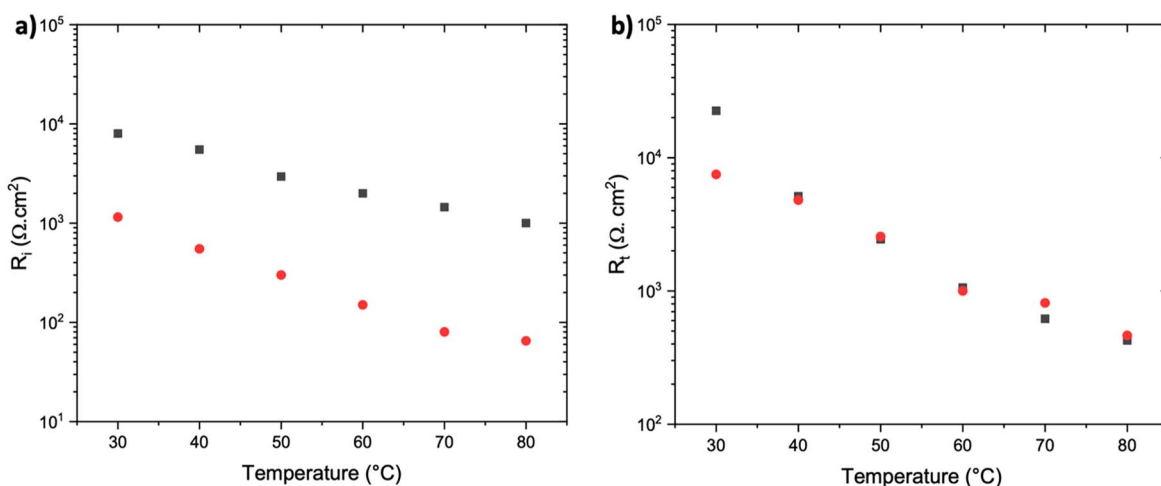


Figure 7. Evolution of the interface resistance (a) R_i and (b) R_i/C_i as a function of temperature for (■) in-situ LiTFSI-Multilayer and (●) ex-situ LiTFSI-Multilayer.

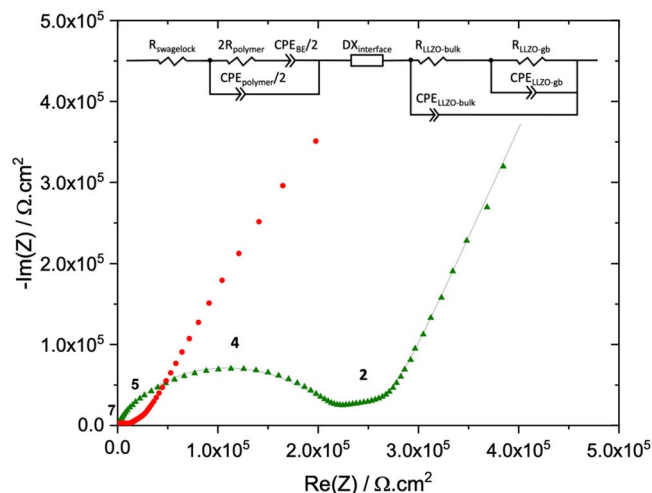


Figure 8. Nyquist plot at 30 °C of (●) ex-situ LiMTFSI—Multilayer, (—) fit according to the equivalent circuit presented and numbers at the data points indicate the power of frequency for ex-situ LiMTFSI—Multilayer and (●) ex-situ LiTFSI—Multilayer.

interactions. In comparison to the study conducted on the LLZTO||PEO—LiTFSI interface ($R_i = 0.2 \text{ k}\Omega\cdot\text{cm}^2$),⁸ the measured value of R_i for our ex-situ LiTFSI—Multilayer ($1.2 \text{ k}\Omega\cdot\text{cm}^2$) at 30 °C is an order of magnitude higher. This discrepancy is likely attributed to a simpler model employed to assess the interface resistance, one that does not fully consider all the heterogeneities (microstructure and chemistry) at the organoclinorganic interface. It is noteworthy that most literature results are obtained at 70 °C, as the conductivities of linear PEO at this temperature ($10^{-3} \text{ S}\cdot\text{cm}^{-1}$) are more suitable for battery applications. Consequently, we compared our R_i values at 70 °C with the literature, revealing a measured value of approximately $0.08 \text{ k}\Omega\cdot\text{cm}^2$. This is two orders of magnitude lower than that reported by Langer et al. ($9 \text{ k}\Omega\cdot\text{cm}^2$ at 70 °C, estimated from the Levie Model) in a symmetrical multilayer cell with LLZO and PEO—LiClO₄.¹⁰

To assess the significance of Li^+ mobility at the interface, the anion was additionally grafted to the polymer chain.¹³ The influence of this modification on interfacial processes, encompassing resistive and/or diffusional phenomena, was examined. To ensure an identical concentration of Li^+ at the interface, we formulated an ex-situ LiMTFSI—Multilayer, incorporating two single-ion polymer membranes synthesized following the method outlined by Naboulsi et al.¹³ The results are gathered in Fig. 8.

First, the impedance spectra are comparable in shape to ex-situ LiTFSI—Multilayers, especially at extremely high and low frequencies. The primary discrepancies arise in the impedance values themselves, and particularly in the MF range, where a distinct shoulder appears, although it is more attenuated and flattened. These impedance differences may be attributed to the significantly higher resistance of the single-ion polymer membrane ($\sim 10^{-7} \text{ S}\cdot\text{cm}^{-1}$) in comparison to the polymer membrane with LiTFSI ($\sim 10^{-5} \text{ S}\cdot\text{cm}^{-1}$). This higher resistance leads to a much more pronounced first semicircle in the HF range.¹³ Using the equivalent circuit presented in Fig. 3c, it is possible to fit the Nyquist plot and the values for R_i and R_t are estimated and gathered in Table SVI.

Figure 9a represents the variation of R_i as a function of the temperature for ex-situ LiTFSI and LiMTFSI. It is evident that, in the ex-situ LiMTFSI—Multilayer, R_i is an order of magnitude higher compared to those observed for the ex-situ LiTFSI—Multilayer. In the case of the ex-situ LiTFSI—Multilayer, the mobility of Li^+ is less restricted compared to the ex-situ LiMTFSI—Multilayer, where the grafting of the anion to the polymer chain alters its mobility.¹³ Interestingly, when examining R_t (Fig. 9b) for the ex-situ LiMTFSI multilayer, it closely compares with the values obtained for the ex-situ LiTFSI multilayer. This suggests that R_t is less impacted by the “bulk” chemical composition. In contrast, R_i appears to be influenced by the chemical composition of the materials in contact and by the energy barrier that Li^+ must overcome when moving from the inorganic to the polymeric phase. In the case of LiTFSI, Li^+ and TFSI⁻ ions are freely distributed within the PEO network, while with LiMTFSI, TFSI⁻ ions are grafted to the PEO network. The disparity in R_i values affirms its close correlation with the concentration of Li^+ ions at the Al—LLZO||PEO network interface.

By examining the temperature-dependent changes in R_i and R_t , we determined the activation energy (E_a) associated with each of these phenomena, considering the assembly processes (Figs. S3 and S4, Table II). We find that the activation energy for R_i is comparable in the case of ex-situ LiTFSI and ex-situ LiMTFSI, showing that the energy barrier for the Li^+ to cross the interface by this shaping process is identical. The polymers are simply held to the surface of the Al—LLZO pellet only by pressure. Conversely, the activation energies for Li^+ differ between in-situ and ex-situ approaches. For R_i , the activation energy is about 0.38 eV for in-situ while it is $\sim 0.54 \text{ eV}$ for the ex-situ one. This suggests that the transport mechanism of Li^+ ions at the interface differs and is easier when the polymer is surface-grafted onto the ceramic. Interestingly, the R_t value is higher in the case of in-situ polymerization compared to the ex-situ one. This indicates that the concentration of Li^+ differs in both situations. For in-situ polymerization, the methacrylate groups

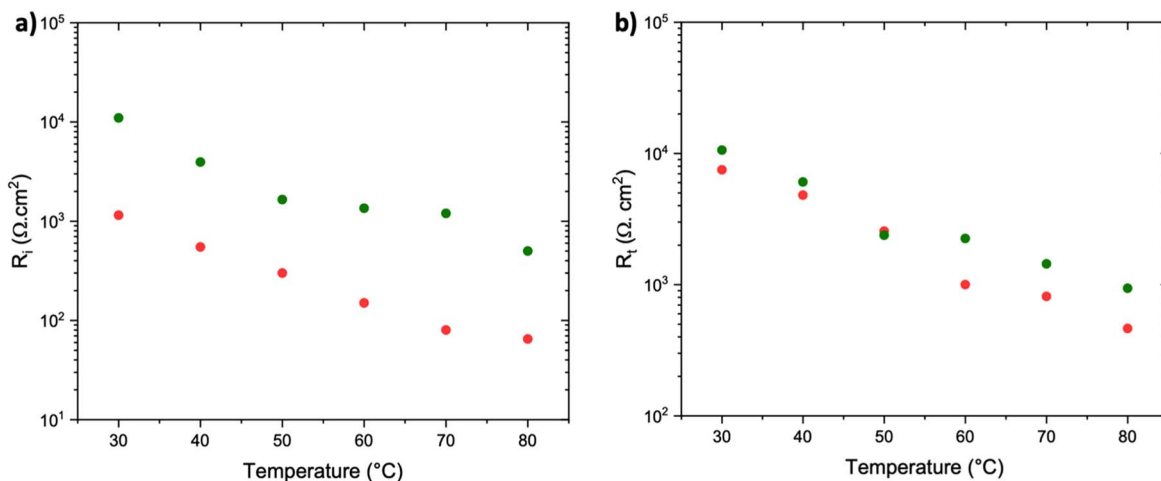


Figure 9. (a) Evolution of the interface resistance (a) R_i and (b) R_t as a function of temperature for (●) ex-situ LiMTFSI—Multilayer and (●) ex-situ LiTFSI—Multilayer.

Table II. Activation energy is estimated for interfacial resistances (R_i and R_t) for the three multilayers.

Sample	E_a (R_i) eV	R^2	E_a (R_t) eV	R^2
in-situ LiTFSI—Multilayer	0.38	0.99	0.60	0.98
ex-situ LiTFSI—Multilayer	0.54	0.99	0.53	0.98
ex-situ LiMTFSI—Multilayer	0.54	0.96	0.43	0.99

reacts with the –OH groups at the Al–LLZO surface, creating an “interphase” that is less favorable to the presence of Li^+ . This contrasts with the ex-situ configuration, where a homogeneous concentration of Li^+ in the membrane is achieved.

The values of R_t remain consistent regardless of how the PEO polymer is assembled at the surface of the ceramics (in-situ vs ex-situ) and the mobility of Li^+ at the interface (whether TFSI is grafted or not), signifying the existence of heterogeneities at the interface. Additionally, the mechanism of Li^+ ion transport at the interface or interphase (in the case of in-situ polymerization) varies, as distinct activation energies (E_a) are measured for different configurations (in-situ LiTFSI, ex-situ LiTFSI, and ex-situ LiMTFSI). This illustrates that regardless of the process used, heterogeneities are present at the interface and influence the indirect transport of Li^+ .

Conclusions

In this paper, we investigated the transport of Li^+ ions across the PEO based network/LLZO interface by designing multilayer structures. Our objective was to understand the motion of Li^+ ions through the composite interphase and identify the physical-chemical parameters that predominantly influence its transport. In this context, we used our knowledge of cross-linked PEO network synthesis from a liquid monomer precursor to examine the impact of grafting the cross-linked PEO network onto the Al–LLZO surface. We also explored the effects of Li^+ mobility at the interface by grafting anions (TFSI) to the PEO chain.

Impedance spectroscopy has been effectively used to evaluate different resistances (polymer, Al–LLZO and interphase) by incorporating an equivalent circuit that includes a TLM element. This model aids in highlighting heterogeneities at the interfaces. Interestingly, we found that R_i , representing the direct transport of Li^+ across the composite interphase, was larger in the case of in-situ polymerization. This may be due to the formation of an interphase with different concentration of Li^+ . On the contrary, the R_t value seems to be unaffected by the method of polymer assembly on the Al–LLZO surface and the manner in which Li^+ is introduced to the PEO network, whether through LiTFSI salts or grafted anions. This resistance is attributed to distribute conductive/insulating zones inside the interphase or interphase (in-situ polymerization) thickness, indicating that this heterogeneity is maintained regardless of the process used. Interestingly, the estimation of activation energy from R_i and R_t confirms the modification of the cross-linked PEO

network/Al–LLZO interface in the case of in-situ polymerization. Specifically, direct Li^+ transport appears to be energetically more favorable.

Acknowledgments

The authors thank RS2E network and DIM-Respire for supporting the AN PhD grant.

ORCID

Christel Laberty-Robert  <https://orcid.org/0000-0003-3230-3164>

References

1. J. Janek and W. G. Zeier, *Nat. Energy*, **1**, 16141 (2016).
2. Y. Zheng, Y. Yao, J. Ou, M. Li, D. Luo, H. Dou, Z. Li, K. Amine, A. Yu, and Z. Chen, *Chem. Soc. Rev.*, **49**, 8790 (2020).
3. Y. Zhao, K. Zheng, and X. Sun, *Joule*, **2**, 2583 (2018).
4. M. Weiss, F. J. Simon, M. R. Busche, T. Nakamura, D. Schröder, F. H. Richter, and J. Janek, *Electrochem. Energ. Rev.*, **3**, 221 (2020).
5. J. Zheng and Y.-Y. Hu, *ACS Appl. Mater. Interfaces*, **10**, 4113 (2018).
6. D. Brogioli, F. Langer, R. Kun, and F. La Mantia, *ACS Appl. Mater. Interfaces*, **11**, 11999 (2019).
7. E. Kuhnert, L. Ladenstein, A. Jodlbauer, C. Slugovc, G. Trimmel, H. M. R. Wilkening, and D. Rettenwander, *Cell Reports Physical Science*, **1**, 100214 (2020).
8. A. Gupta and J. Sakamoto, *Electrochem. Soc. Interface*, **28**, 63 (2019).
9. J. A. Isaac, L. R. Mangani, D. Devaux, and R. Bouchet, *ACS Appl. Mater. Interfaces*, **14**, 13158 (2022).
10. F. Langer, M. S. Palagonia, I. Bardenhagen, J. Glenneberg, F. La Mantia, and R. Kun, *J. Electrochem. Soc.*, **164**, A2298 (2017).
11. R. De Levie, *Electrochim. Acta*, **10**, 113 (1965).
12. F. La Mantia, J. Vetter, and P. Novák, *Electrochim. Acta*, **53**, 4109 (2008).
13. A. Naboulsi, R. Chometon, F. Ribot, G. Nguyen, O. Fichet, and C. Laberty-Robert, (2023), ACS Applied Materials & Interfaces. Under revision.
14. L. Porcarelli, A. S. Shaplov, F. Bella, J. R. Nair, D. Mecerreyes, and C. Gerbaldi, *ACS Energy Lett.*, **1**, 678 (2016).
15. S. Chen, J. Wang, Z. Wei, Z. Zhang, Y. Deng, X. Yao, and X. Xu, *J. Power Sources*, **431**, 1 (2019).
16. W. Nonnenmacher and J. Euler, *Electrochim. Acta*, **2**, 268 (1960).
17. A. Sharafi, S. Yu, M. Naguib, M. Lee, C. Ma, H. M. Meyer, J. Nanda, M. Chi, D. J. Siegel, and J. Sakamoto, *J. Mater. Chem. A*, **5**, 13475 (2017).
18. H. Huo, J. Luo, V. Thangadurai, X. Guo, C.-W. Nan, and X. Sun, *ACS Energy Lett.*, **5**, 252 (2020).
19. M. E. Orazem, I. Frateur, B. Tribollet, V. Vivier, S. Marcelin, N. Pébère, A. L. Bunge, E. A. White, D. P. Riemer, and M. Musiani, *J. Electrochem. Soc.*, **160**, C215 (2013).
20. J. T. S. Irvine, D. C. Sinclair, and A. R. West, *Adv. Mater.*, **2**, 132 (1990).
21. H. Nara, D. Mukoyama, T. Yokoshima, T. Momma, and T. Osaka, *J. Electrochem. Soc.*, **163**, A434 (2016).